Electronic Supplementary Material (ESI) for Journal of Materials Chemistry C.
This journal is © The Royal Society of Chemistry 2024

Supplementary Information

Facile In-situ Synthesis of Double Perovskite $Cs_2AgBiBr_6/WS_2$ Heterostructure and Interfacial Charge Transfer Mediated High-Performance Ultraviolet Photodetection

Ravinder Chahal[1], Abdul Kaim Mia[2], Abhilasha Bora[2], and P. K. Giri[1*]

[1]Department of Physics, Indian Institute of Technology Guwahati, Guwahati, Assam 781039

[2]Centre for Nanotechnology, Indian Institute of Technology Guwahati, Guwahati, Assam 781039

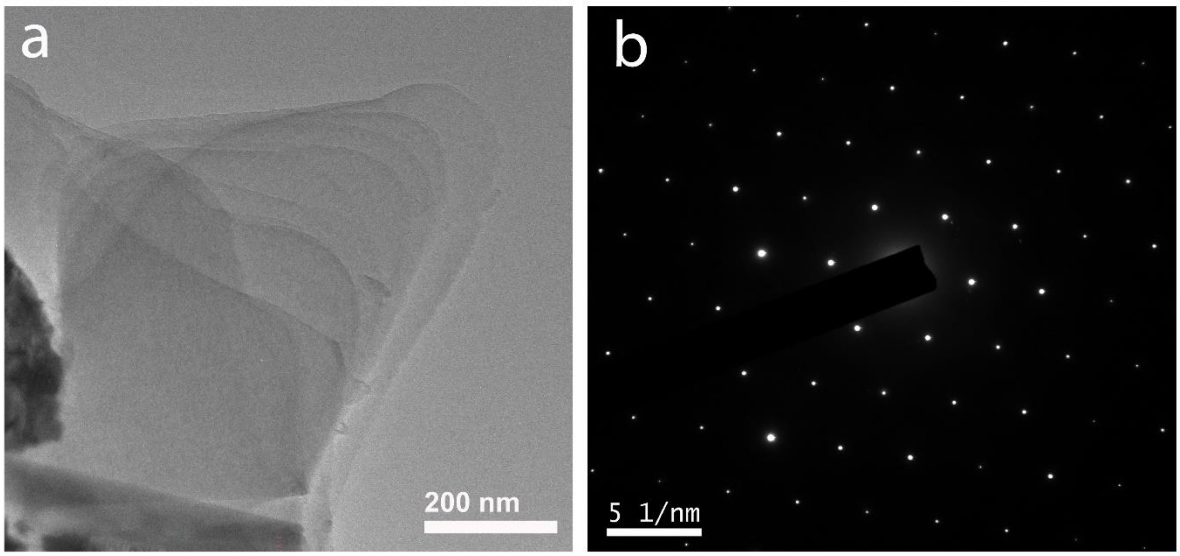

Figure S1. (a) FETEM image of multi-layer WS_2 nanosheets prepared by ultrasonication method. **(b)** The corresponding selected area electron diffraction pattern of WS_2 nanosheets.

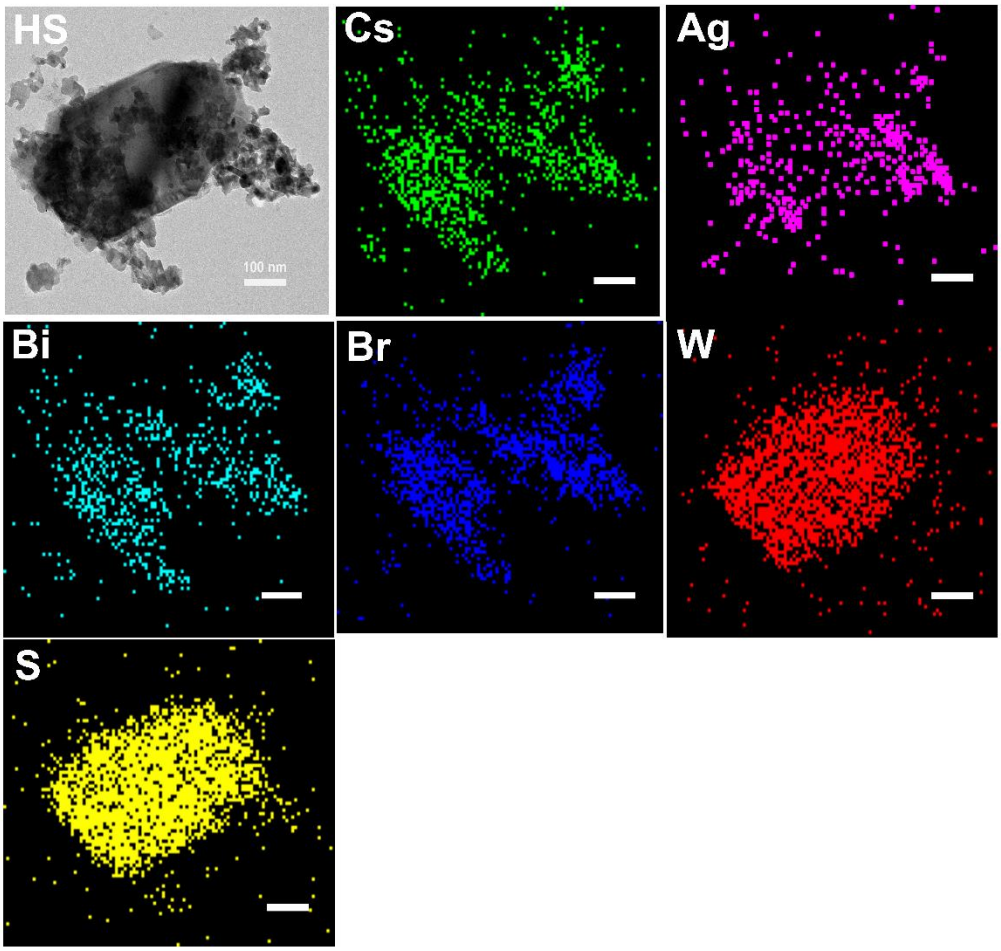

Figure S2. (a) FETEM image of the $Cs_2AgBiBr_6/WS_2$ heterostructure. **(b-g)** Elemental mapping of Cs, Ag, Bi, Br, W, and S elements in $Cs_2AgBiBr_6/WS_2$ heterostructure, respectively. The scale bar in each image is 100 nm.

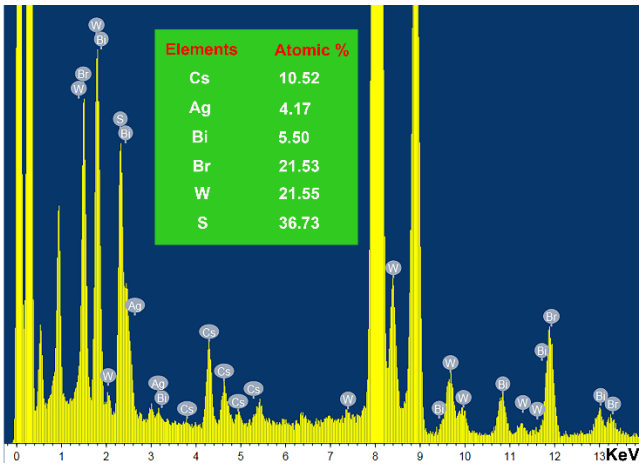

Figure S3: The corresponding TEM-EDX spectra of DP/WS_2 heterostructure.

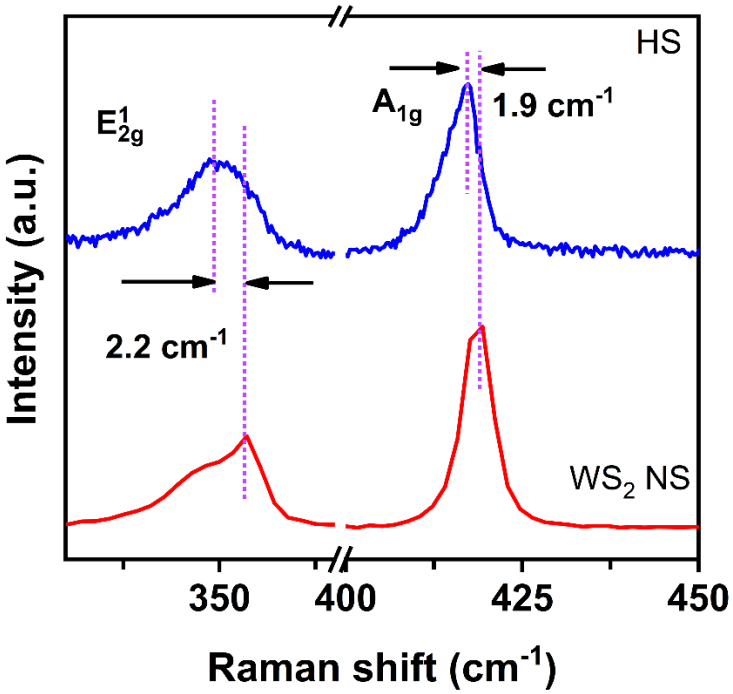

Figure S4. Comparison of the Raman spectra of WS_2 (red) and $Cs_2AgBiBr_6/WS_2$ (blue) heterostructure.

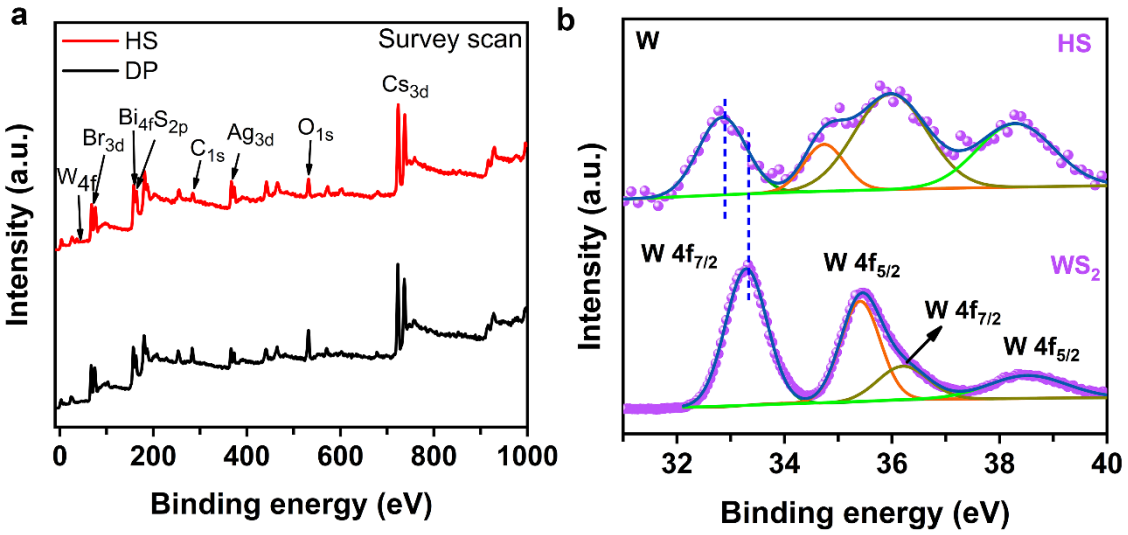

Figure S5. (a) XPS survey scan spectra of $Cs_2AgBiBr_6$ DP (black) and $Cs_2AgBiBr_6/WS_2$ heterostructure (red). **(b)** Comparison of high-resolution XPS spectra of tungsten (W) in WS_2 nanosheets and $Cs_2AgBiBr_6/WS_2$ heterostructure.

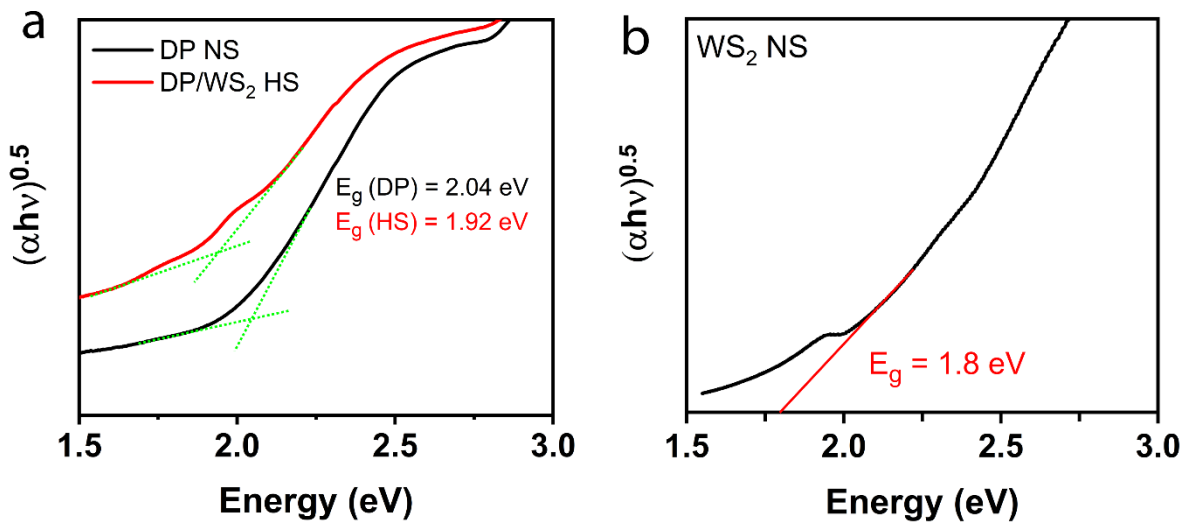

Figure S6. (a) Tauc plot of $Cs_2AgBiBr_6$ DP (black) and $Cs_2AgBiBr_6/WS_2$ heterostructure (red). The green dotted line displays the linear fitting of the graphs. **(b)** Tauc plot of the few-layer WS_2 nanosheets (black). The red line is the linear fitting of the graph.

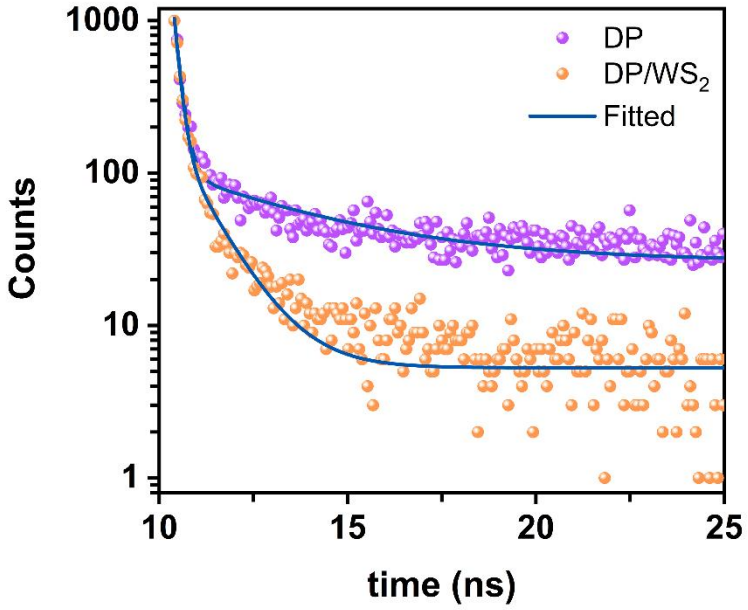

Figure S7. Time-resolved PL spectra of $Cs_2AgBiBr_6$ DP (magenta) and $Cs_2AgBiBr_6/WS_2$ heterostructure (orange). The solid blue line represents exponential fitting.

Table S1: TRPL decay parameters of $Cs_2AgBiBr_6$ DP and $Cs_2AgBiBr_6/WS_2$ HS.

Sample	A_1	τ_1 (ns)	A_2	τ_2 (ns)	τ_{avg} (ns)
$Cs_2AgBibr_6$ DP	2.4	0.16	7.3	3.7	3.65
$Cs_2AgBiBr_6$ DP/ WS_2 (HS)	3.5	0.14	2.8	0.95	0.82

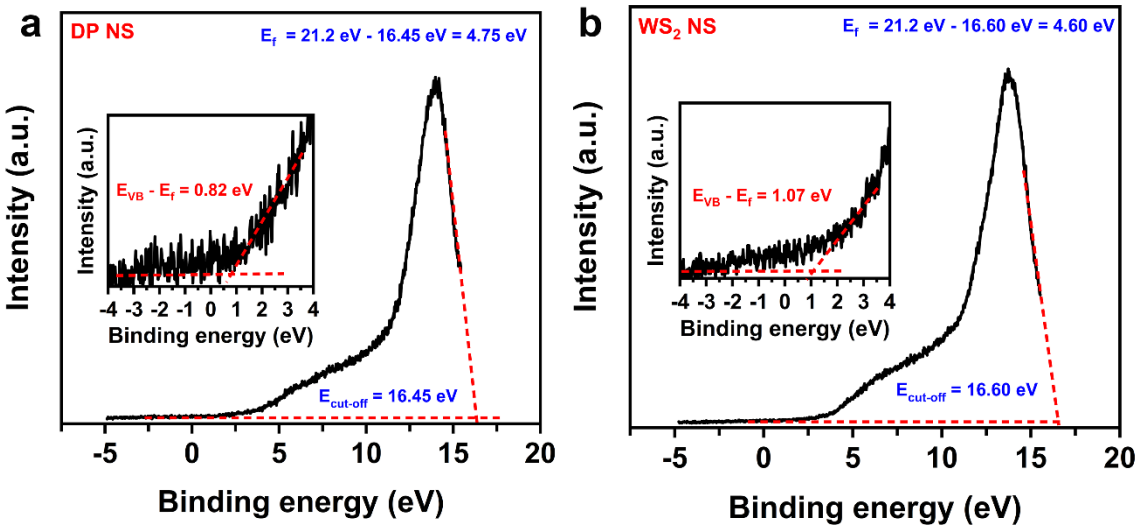

Figure S8. UPS spectra of **(a)** $Cs_2AgBiBr_6$ DP, and **(b)** WS_2 nanosheets. The inset in each case shows the magnified view of the plot in the lower binding energy region.

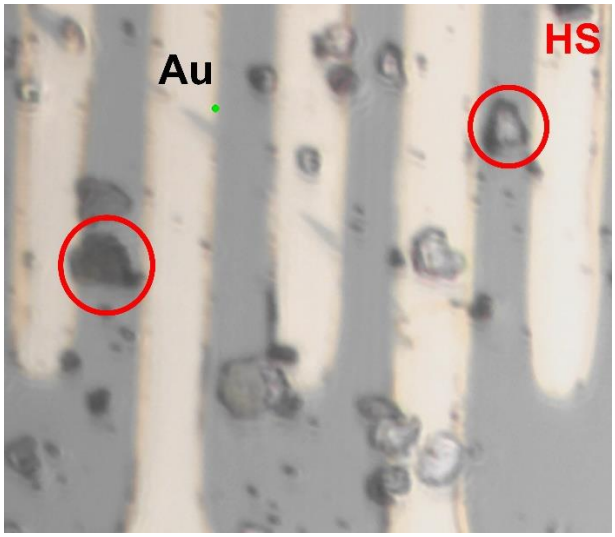

Figure S9. The real-time image of the $Cs_2AgBiBr_6/WS_2$ heterostructure photodetector.

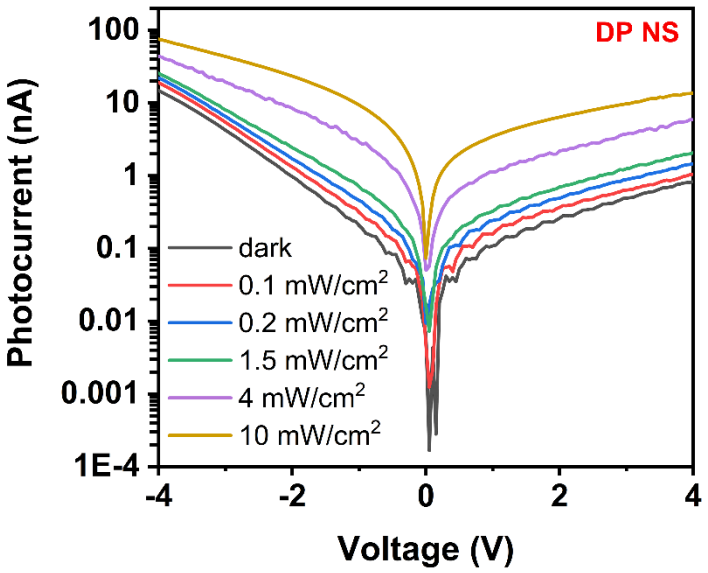

Figure S10. I-V characteristics of $Cs_2AgBiBr_6$ DP with varying incident laser power.

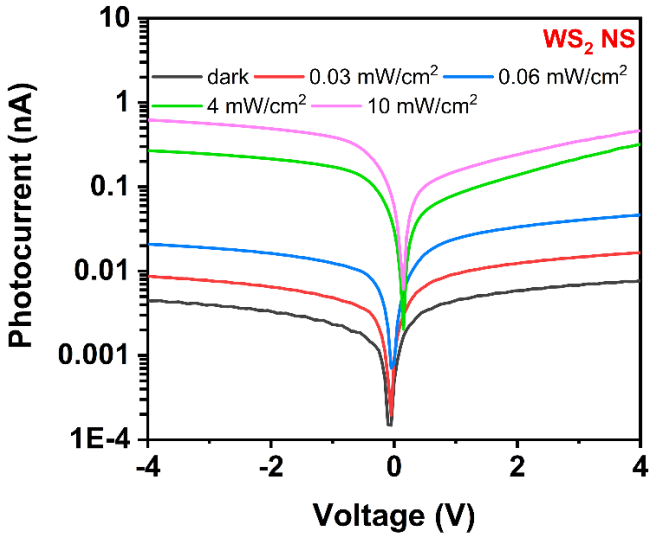

Figure S11. Dark and photo I-V characteristics of WS_2 nanosheets with different intensity laser illumination.

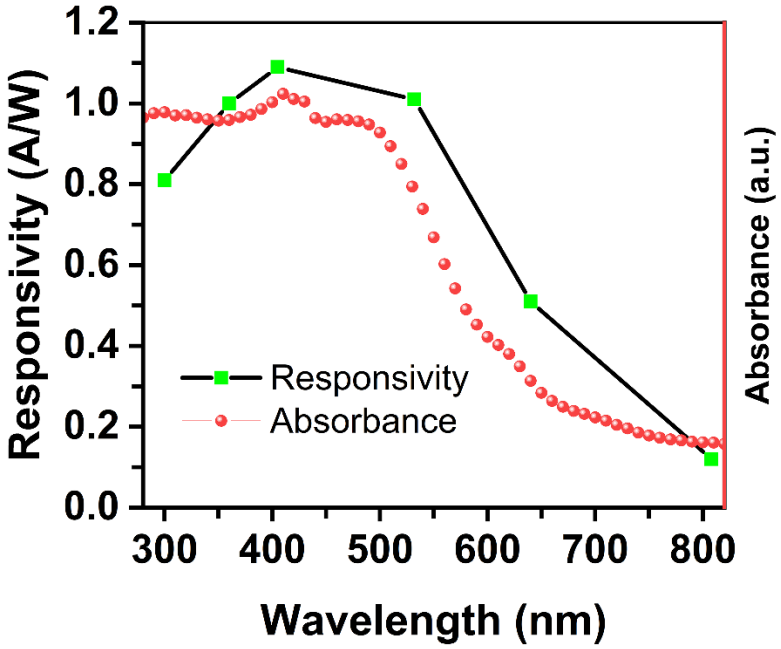

Figure S12. Wavelength-dependent Responsivity and absorption spectra of DP/WS_2 heterostructure.

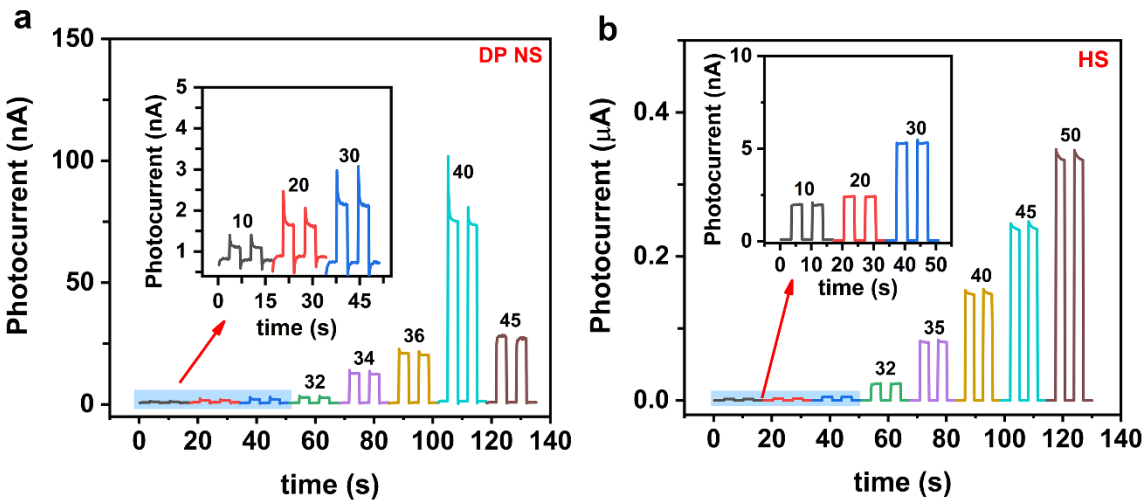

Figure S13. (a) Photocurrent response of $Cs_2AgBiBr_6$ DP with different laser power (mW). **(b)** Photocurrent response of $Cs_2AgBiBr_6/WS_2$ heterostructure with varying incident laser powers for 405 nm diode laser.

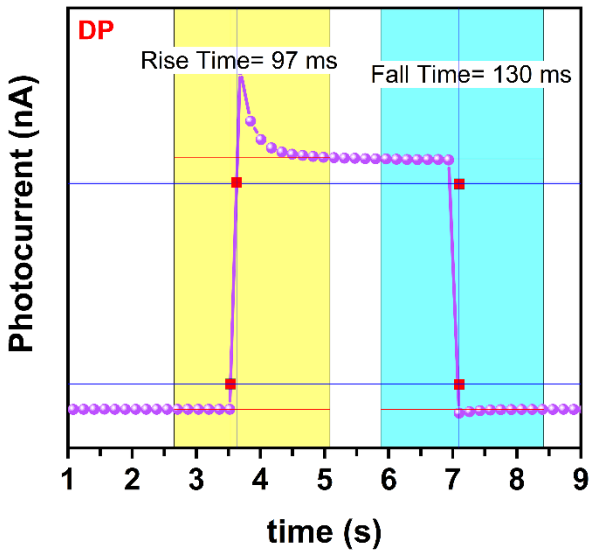

Figure S14. Photocurrent rise and fall time profiles of $Cs_2AgBiBr_6$ DP with pulsed laser excitation.